CHEMISTRY OF MATERIALS

pubs.acs.org/cm

Article

Ammonia Capture via an Unconventional Reversible Guest-Induced Metal-Linker Bond Dynamics in a Highly Stable Metal−Organic Framework

Pengbo Lyu,[¶] Ashley M. Wright,[¶] Alfredo López-Olvera,[¶] Paulo G.M. Mileo, J. Antonio Zárate, Eva Martínez-Ahumada, Vladimir Martis, Daryl R. Williams, Mircea Dincă,* Ilich A. Ibarra,* and Guillaume Maurin*

Cite This: *Chem. Mater.* 2021, 33, 6186−6192

Read Online

ACCESS | Metrics & More | Article Recommendations | Supporting Information

ABSTRACT: An unprecedented reversible guest-induced metal-linker bond rearrangement in metal−organic framework (MOFs) was revealed by quantum-calculations and DRIFT experiments. As a showcase, the prototypical MOF-type MFM-300(Sc) was demonstrated to undergo a substantial Sc-carboxylate bond dynamics upon ammonia adsorption to enable a strong metal−guest binding mode, a key feature to ensure a highly efficient capture of this toxic molecule. Decisively, we evidenced this adsorption mechanism to be fully reversible, preserving the ammonia capture performance and structure integrity over multiple cycles. Such an unconventional mechanism in MOFs can open up new avenues to design novel materials for an efficient capture of highly corrosive molecules.

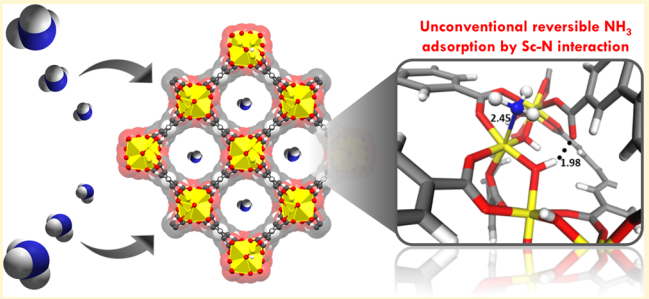

1. INTRODUCTION

Metal−organic frameworks (MOFs), one of the most prominent classes of porous materials, initially suffered from poor chemical stability, a key issue that limited their use in many applications. Huge efforts have been thus devoted over the last decade to design highly stable MOFs mostly by reinforcing the metal-linker coordination bond via the combination of high-valence metal (III/IV) and highly complexing ligands (carboxylate, phenolate, and triazole) or low-valence metal (II) and azolate linkers.[1−3] Because these coordination bonds are strong, this generally leads to a misconception that they are static excluding their potential flexibility/dynamics up to the point of being labile.[4−6]

Reversible metal-linker bonding, for example, dynamic, adaptable, stimuli-responsive, and self-healing bonding,[7−9] has only been recently introduced to explain key phenomena in MOFs from their crystal growth to their phase transitions.[10] Typically, Bennett and Horike have intensively explored the concept of metal-linker dynamics to understand the melting mechanisms of ZIF liquids and glasses.[11−13] Very recently, Brozek et al.[14] reported a cornerstone investigation of the metal-linker dynamics in a set of carboxylate MOFs, for example, HKUST-1, MOF-5, and MOF-74, through variable-temperature diffuse reflectance infrared Fourier transform spectroscopy (VT-DRIFTS) coupled with molecular simulations. These authors challenged the conception of carboxylate MOFs as static structures demonstrating that the metal-carboxylate bonds exist in equilibrium between "tight" and "loose" states corresponding to short (strong) and long (weak) range interactions, respectively, where the use of high temperature favors the loose states.[15,16]

So far, the perception of metal-linker dynamics has been almost exclusively evidenced with the use of temperature as the external stimulus as well as during the SBU cation/ligand exchanges.[11−13,15,16] Undoubtedly, a wider range of stimuli are worth investigating to expand the horizons of this research line in the field of MOFs. In particular, are guest molecules able to trigger such bond reorganization in a reversible manner? To the best of our knowledge, such a guest-assisted phenomenon has been only revealed by an earlier work reported in 2011 by Kitawaga et al.[17] This group demonstrated a reversible metal−ligand bond rearrangement of a Zn-paddle-wheel MOF upon CO_2 adsorption at low pressure. Indeed, the exploration of metal-linker lability is of utmost importance not only to better understand phase transitions but also to unravel uncommon adsorption mechanisms. This is a keystone to pave the way toward the development of MOFs to capture highly corrosive

Received: May 28, 2021
Revised: July 12, 2021
Published: July 27, 2021

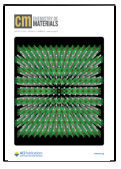

https://doi.org/10.1021/acs.chemmater.1c01838
Chem. Mater. 2021, 33, 6186−6192

contaminants such as H_2S, SO_X, NO_X, and NH_3, which are known to challenge the robustness of MOFs.[5,18−22] Specifically, ammonia capture by MOFs has been intensively explored over the last decade.

Herein, we report an alternative NH_3 adsorption mechanism in the carboxylate MOF MFM-300(Sc) that implies an unprecedented fully reversible guest-induced metal-linker bond rearrangement as revealed by periodic density functional theory (DFT) calculations and further confirmed by DRIFT experiments. A NH_3-triggered Sc−O loose state is first created that initiates a metal-carboxylate bond lability to promote a Sc−N(NH_3) coordination mode, while the free pending carboxylate group is stabilized by hydrogen bond with the neighbor μ-OH group. Remarkably, this unconventional adsorption phenomenon involving strong host/guest interactions was demonstrated to ensure a fully reversible ammonia capture with only a small hysteresis loop in the adsorption and desorption isotherms while maintaining the structure integrity of the MOF framework. MFM-300(Sc),[23] isostructural to the −Al[24] and −In, −Fe, −V, and −Cr analogues,[25] comprises of [$ScO_4(OH)_2$] nodes bridged by 3,3′,5,5′-biphenyl-tetracarboxylate (BPTC) linkers to form a wine-track channel of 8.1 Å with μ-OH groups pointing toward the pore (Figures 1 and S1).[26] MFM-300(Sc) has demonstrated promising adsorption performance toward a series of molecules, for example, H_2,[23] CO_2,[27] CH_4,[27] SO_2,[28] H_2S,[29] I_2,[30] H_2O,[31] and ferulate[32] combined with a high stability in diverse media.

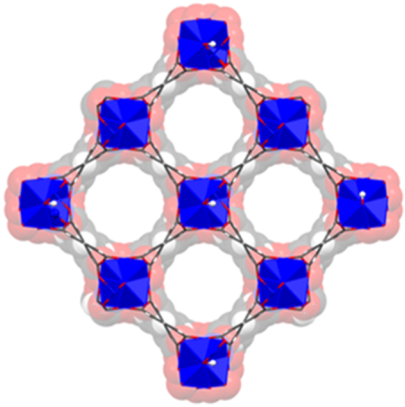

Figure 1. View along the *c*-axis of pore channels of MFM-300(Sc).

2. EXPERIMENTAL METHODS

MFM-300(Sc) was synthesized according to a previously reported method.[23]

Scandium triflate (0.030 g, 0.061 mmol) and H_4BPTC (0.010 g, 0.030 mmol) were mixed in THF (4.0 mL), DMF (3.0 mL), water (1.0 mL), and HCl (36.5%, 2 drops). The resultant slurry mixture was stirred until complete dissolution occurred. The solution was then placed in a pressure tube and heated in an oil bath to 75 °C for 72 h. The tube was cooled down to room temperature at a rate of 0.1 °C/min, and the colorless crystalline product was separated by filtration, washed with DMF (5.00 mL), and dried in air.

Powder X-ray diffraction (PXRD) patterns were recorded with a Bruker Advance II diffractometer equipped with a $\theta/2\theta$ Bragg−Brentano geometry and Ni-filtered Cu Kα radiation (Kα^1 = 1.5406 Å, Kα^2 = 1.5444 Å, Kα^1/Kα^2 = 0.5). The tube voltage and current were 40 kV and 40 mA, respectively. Samples for PXRD were prepared by placing a thin layer of the appropriate material on a zero-background silicon crystal plate.

Nitrogen adsorption isotherms were measured by a volumetric method using a Micromeritics ASAP 2020 gas sorption analyzer. The sample mass was 65.0 mg. Free space correction measurements were performed using ultrahigh purity He gas (UHP grade 5, 99.999% pure). Nitrogen isotherms were measured using UHP grade Nitrogen. All nitrogen analyses were performed using a liquid nitrogen bath at 77 K. Oil-free vacuum pumps were used to prevent contamination of the sample or feed gases.

Ammonia adsorption isotherms were measured by a volumetric method using a Micromeritics ASAP 2020 gas sorption analyzer fitted with Kalrez seals. An empty tube fitted with a Micromeritics TranSeal was initially weighed and filled with the unactivated sample. After activation on the degas port at 160 °C for 18 h, the mass of the tube and sample was reweighed, and the initial mass was subtracted resulting in a mass of 65.0 mg of the activated material. Free space correction measurements were performed using ultrahigh purity He gas (UHP grade 5, 99.999% pure). Ammonia isotherms were measured using UHP grade ammonia. All ammonia analyses were performed using water baths held at constant temperature with a recirculating chiller. Oil-free vacuum pumps were used to prevent contamination of the sample or feed gases.

DRIFTS spectra were performed using an FTIR Nicolet 6700 spectrophotometer (DTGS detector) with a 4 cm^{-1} resolution equipped with a diffuse reflectance vacuum chamber with CaF_2 windows. The FTIR spectra of the activated samples of MFM-300(Sc) were collected (8×10^{-6} bar and 180 °C for 6 h) under an atmosphere of NH_3 with an increase of NH_3 pressure from 0.06 to 0.24 bar, and after NH_3 adsorption.

Thermal gravimetric analysis (TGA) was performed using a TA Instruments Q500HR analyzer, under a N_2 atmosphere in the high-resolution mode (dynamic rate TGA) at a scan rate of 2 °C/min, from room temperature to 640 °C.

3. RESULTS AND DISCUSSION

PXRD and TGA were used to confirm the phase purity of the synthesized MFM-300(Sc) material (Figures S2−S3). An acetone-exchanged sample was fully evacuated at 453 K and 1.7×10^{-3} Torr for 6 h, and its resulting BET area (1365 m^2 g^{-1}) and pore volume (0.56 cm^3 g^{-1}) (Figure S4) were in excellent agreement with the theoretical values (1390 m^2 g^{-1} and 0.58 cm^3 g^{-1}, respectively).

The NH_3 adsorption−desorption isotherms were collected for this activated sample at 298 K up to 1 bar. The resulting adsorption isotherm exhibits a very steep initial rise followed by a step change above 0.03 bar with NH_3 uptake increasing almost linearly up to 13.1 mmol g^{-1} at 1 bar (Figures 2 and S5−S6). The strong affinity of MFM-300(Sc) to NH_3 was supported by the high isosteric heat of adsorption (Q_{st}) calculated at a low coverage of ∼48.3 kJ mol^{-1} (Figures S7 and S8). This value is comparable to those of other relevant MOFs, for example, Co_2Cl_2BTDD,[20] MFM-300 (M = V^{IV} and Cr),[21] and CPM-110b[22] among others (see Table S4). Furthermore, the desorption branch revealed a hysteretic reversible adsorption process while PXRD confirmed the structural integrity of MFM-300(Sc) after exposure to NH_3 (Figures S9 and S10). Moreover, this adsorption/desorption behavior is maintained over multiple cycles, strongly supporting a fully reversible capture/release mechanism (Figures 2 and S11).

Intriguingly, although MFM-300(Sc) shows a similar NH_3 uptake capacity at 1 bar to its Al-analogue[24] (13.9 mmol g^{-1} at 293 K), the shape of its adsorption isotherm deviates from the I-type profile exhibited by the former material (Figure S12).[24] The presence of an abnormal low-pressure step change with a loading of ∼1 NH_3 molecule per μ-OH group prompted us to conduct an in-depth exploration of the adsorption mechanism. Force field-based Monte Carlo simulations (Supporting

https://doi.org/10.1021/acs.chemmater.1c01838
Chem. Mater. 2021, 33, 6186−6192

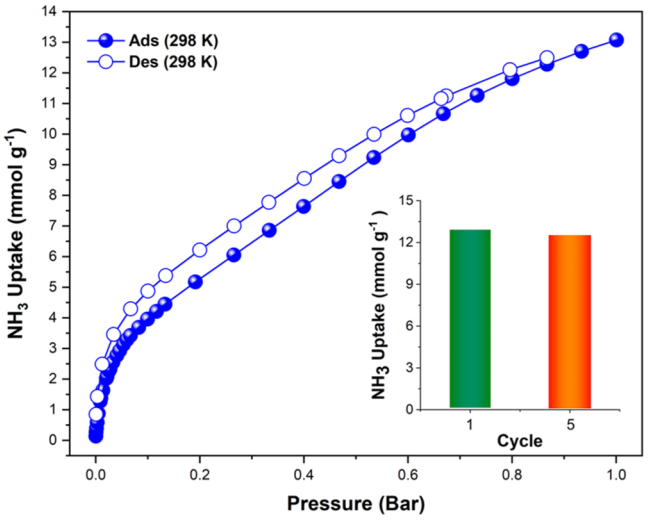

Figure 2. Experimental NH_3 adsorption−desorption isotherms collected for a fully activated MFM-300(Sc) sample (filled blue circles = adsorption; open blue circles = desorption) at 298 K and up to 1 bar. Inset: comparison of NH_3 uptake of MFM-300(Sc) from the first and fifth adsorption cycles (13.1 and 12.6 mmol g^{-1}, respectively. Corresponding to a decrease of 3.8%) at 298 K and up to 1 bar.

Information and Figure S13 for computational details) first revealed that the interactions between NH_3 and the μ-OH groups with a mean separating N(NH_3)−H(μ-OH) distance of 2.23 Å as reported in the corresponding radial distribution plot (Figure S14) dominate the initial stage of adsorption. However, the resulting adsorption enthalpy calculated at low coverage (36 kJ mol^{-1}) as well as the DFT-derived adsorption energy associated with this preferential binding site (40 kJ mol^{-1}) are both significantly lower than the Q_{st} value (48.3 kJ mol^{-1}). Therefore, this standard NH_3/μ-OH adsorption mode cannot account entirely for the adsorption behavior of MFM-300(Sc) in the low-pressure regime. This is also supported by the deviation between the experimental and the grand canonical Monte Carlo simulated adsorption isotherms in both low- and intermediate-pressure ranges (Figure S14). Periodic DFT calculations were thus performed to envisage alternative NH_3 adsorption modes in MFM-300(Sc). To that purpose, because the interaction energy for NH_3 was found to be higher as compared to many other gas molecules (Figure S15 and Table S5), we deliberately envisaged a possible reaction path involving a metal-carboxylate bond dynamics upon NH_3 adsorption as illustrated in Figure 3. In this scenario, this reaction path starts with an initial state (IS), where NH_3 is adsorbed to the μ-OH site (Figure S15). Our climbing image nudged elastic band (CI-NEB) calculations revealed the existence of an intermediate state (INT), where the guest molecule relocates from the μ-OH site to a neighbor Sc atom and induces an elongation of one Sc−O bond from 2.14 Å (IS) to 2.22 Å (INT) (see Figure 2). This local structure reorganization occurring throughout a first transition state (TS1) is reminiscent of the thermal-driven loose state for a metal-carboxylate bond very recently demonstrated for some typical MOFs.[14] Following up, the Sc−O bond completely breaks, and the resultant dangling O-atom establishes a hydrogen-bond type interaction (associated O−H distance of 1.88 Å) with the neighbor μ-OH group as observed in the second transition state (TS2). Interestingly, this guest-triggered labile Sc-carboxylate bonding enables the NH_3 to coordinate to the Sc via its N-atom with a corresponding bond distance of 2.45 Å in the final state (FS), which is similar to the Sc−N bond length observed in a related complex.[33] The associated energy barriers for the two steps (40 and 25 kJ mol^{-1} for TS1 and TS2, respectively) are relatively moderate, which makes this uncommon guest-induced dynamic metal-linker bonding thermodynamically feasible. Ab initio molecular dynamics (AIMD) simulations performed at 400 K further confirmed that such resulting Sc-NH_3 coordinative mode (FS) remains stable over time, which means that this corresponds to an energetically favorable configuration (Figure S16).

Interestingly, further AIMD calculations evidenced that once NH_3 is removed from the FS configuration, the MOF framework is self-healed, and its initial crystal structure is regenerated (Figure S16). Therefore, this NH_3-triggered dynamic metal-linker bonding is demonstrated to be fully reversible, which accounts for the experimentally observed adsorption/desorption behavior of MFM-300(Sc). Remarkably, the FS → IS process occurs fast in the AIMD simulations (about 1 ps) in line with the very low energy barriers required to recover INT and IS states starting from FS (29 and 4 kJ mol^{-1} respectively) as shown in Figure 3. This result suggests an easy regeneration of MFM-300(Sc) after NH_3 adsorption

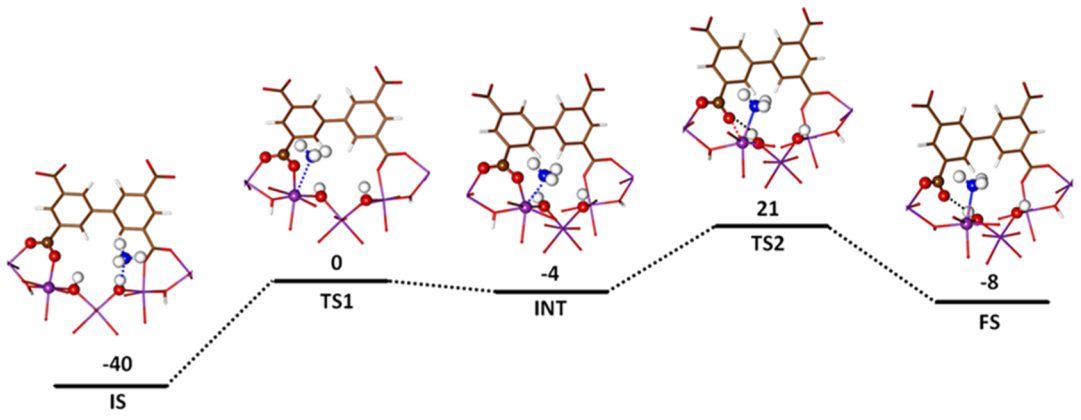

Figure 3. DFT-simulated potential energy profile for the NH_3-triggered Sc-carboxylate dynamic bonding in MFM-300(Sc) and illustrations of the initial state (IS), transition states (TS1 and TS2), intermediate state (INT), and final state (FS). Color code: carbon (brown), oxygen (red), nitrogen (blue), hydrogen (white), and scandium (purple). The distances and potential energies are reported in Å and in kJ mol^{-1} respectively. The key distances (Sc−N and Sc−O) are summarized in Table S6.

https://doi.org/10.1021/acs.chemmater.1c01838
Chem. Mater. 2021, 33, 6186−6192

consistent with the small hysteresis exhibited by the desorption branch. Moreover, such a predicted bond rearrangement enables the optimization of the MOF/NH_3 affinity because the interaction energy associated with the binding mode of NH_3 toward the created open-metal site is significantly higher as compared to the NH_3/μ-OH adduct (Table S5). This is also reflected in the charge difference plots reported in Figure 4 for

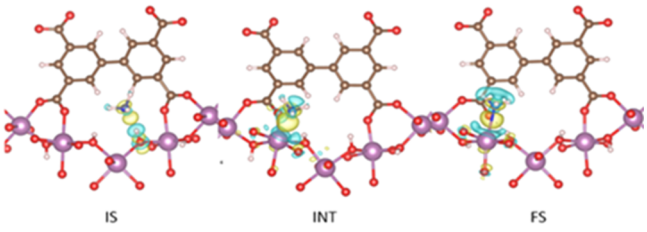

Figure 4. DFT-derived charge differences for the adsorption of NH_3 in IS, INT, and FS with an isovalue of ±0.002 e Å^{-3}; yellow and cyan colors represent the charge accumulation and depletion regions, respectively. The color code for all atoms is the same as Figure 2.

IS, INT, and FS. We can observe that the charge significantly accumulates between Sc and NH_3 molecules in INT and FS, while both charge accumulation and the depletion region coexist between μ-OH and NH_3 in IS. This uncommon reversible dynamics of this soft porous crystal is a key feature to make it as an optimal candidate for NH_3 capture.

This mechanistic investigation revealed that the unusual Sc–NH_3 binding mode requires the formation of the INT state. As a showcase, we further replaced Sc by Al in this INT structure and a DFT-geometry optimization was performed. The optimized structure reported in Figure S17 indicates that the NH_3 does not remain bound to the metal, Al readopting its pristine $AlO_4(OH)_2$ octahedral environment. Therefore, this calculation strongly suggests that MFM-300(Al) cannot exhibit such NH_3-triggered bond dynamics in line with its different profile for the adsorption isotherm at low pressure as discussed above.

To confirm this predicted NH_3 adsorption mechanism, in situ DRIFT spectroscopy experiments were further carried out at 298 K, as a qualitative relationship between the intensity of bands and the ammonia adsorbed into MFM-300(Sc).[34−36] Figures 5 and S18 and S19 report the corresponding IR spectra, split into distinct wavelength regions, recorded for the pristine sample exposed to a gradual increase of NH_3 pressure from 0.06 (the allowed detection limit of the instrument) to 0.24 bar. We first observed that the intensity of the two bands at 1351−1318 cm^{-1} attributed to the symmetric and degenerate deformation modes of NH_3, respectively,[34−36] increases gradually with pressure (Figure S19). This trend is consistent with a progressive filling of the MOF pores. Figure 5a shows characteristic bands at 1740 and 1727 cm^{-1} corresponding to symmetric and asymmetric COO^- stretching mode, respectively,[35,37−39] their intensity increases progressively upon NH_3 adsorption. This is associated with the formation of free pending C═O groups that results from the metal-linker bond breaking as predicted for FS in Figure 3. A similar spectroscopic signature was previously evidenced by Bandosz and Petit for HKUST-1[40,41] and MOF-5.[42] The bands related to the COO^- stretching mode drastically changed when these two MOFs exposed to toxic gases, for example, NH_3, H_2S, and NO_2 suffered from a partial or a full metal-carboxylate bond breaking, leading to the formation of free C═O groups as detected by the bands at 1650−1710 cm^{-1}. The perturbation in symmetric−asymmetric carboxylate stretching frequency can also be related to a possible transition from *syn*−*syn* (parallel bidentate bridging) to monodentate carboxylate binding.[43]

Figure 5b reveals the presence of two bands at 827 and 840 cm^{-1}. According to the literature, the first band corresponds to the Sc−O stretching mode.[44−46] Despite the lack of literature on comprehensive FTIR experimental characterization of the Sc(III)−N interactions, we assigned the second band at 840 cm^{-1} to the Sc(III)−N rocking vibrational mode by analogy with previous FTIR investigations on hexa-coordinated ammine-trivalent metal complexes including $[Rh(NH_3)_6]Cl_3$, $[Os(NH_3)]Br_3$, $[Ir(NH_3)_6]Cl_3$, $[Cr(NH_3)_6]^{3+}$, and $[Co(NH_3)_6]Cl_3$ as reported by Griffith,[47] Quagliano,[48] and Gupta.[49] These authors demonstrated that the M(III)−N rocking vibrational mode appears in the range of 740−860 cm^{-1}.

The band assigned to the O−H stretching mode of the μ-OH group in the 3800−3600 cm^{-1} range was shown to undergo a broadening and a reduction in intensity upon NH_3 adsorption (Figure 5c). Such evolution of the band indicates that μ-OH progressively forms hydrogen bonds as reported previously for ammonia adsorbed in the MFM-300(Al) analogue and M-PMOFs.[24,50] It is well established that the bands at 950 and 1628 cm^{-1} associated with the symmetric and asymmetric bending $\delta(N-H_x)$ modes of NH_3 are shifted to 1150−1100 and 1630 cm^{-1} when this molecule forms a hydrogen bond with a OH group.[35,51] However, Figure S19

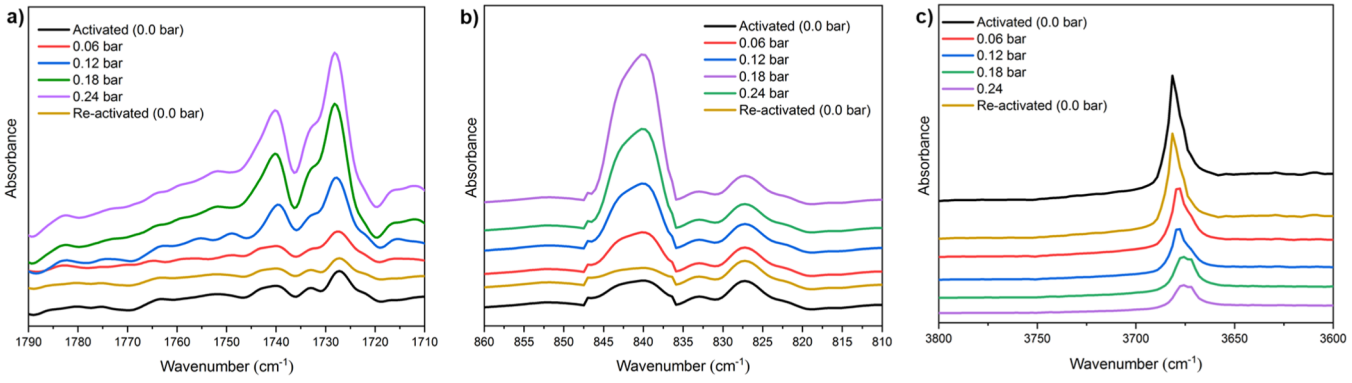

Figure 5. DRIFT spectra of NH_3 adsorbed at different pressures (from 0 to 0.24 bar) over activated MFM-300(Sc) at 298 K, split into three wavelength regions: (a) 1790−1710 cm^{-1}; (b) 860−810 cm^{-1}, and (c) 3800−3600 cm^{-1}.

https://doi.org/10.1021/acs.chemmater.1c01838
Chem. Mater. 2021, 33, 6186−6192

does not show any band in this region. Taking into consideration that the bands at 1740 and 1727 cm^{-1} (Figure 5a) did not show any shift to lower frequency as typically observed for monodentate carboxylate species,[25] and we only observed changes in their intensity, the broadening of the band at 3683 cm^{-1} (μ-OH stretching) was attributed to the formation of a hydrogen bond between the μ-OH group and the free pending carboxylate group as previously observed.[48,49,52] Altogether, these in situ DRIFT data allow a validation of the predicted NH_3 adsorption mode (FS) as reported in Figure 3. Moreover, we evidenced that starting with the NH_3-loaded sample at 0.24 bar and applying a vacuum of 1.7×10^{-3} Torr lead to a full recovery of the IR spectrum collected for the pristine sample. This observation clearly confirms the reversibility of the adsorption process.

4. CONCLUSIONS

In summary, quantum-calculations supported by DRIFT experiments demonstrated that MFM-300(Sc) exhibits an unprecedented fully reversible NH_3-induced metal-linker bond rearrangement. This unconventional adsorption mechanism enables a strong binding of NH_3 toward the created Sc open metal sites while preserving the ammonia capture performance and crystal structure of the MOF over multiple cycles. This key finding provides new horizons on the understanding of the complex adsorption mechanism and paves the way toward further developments of MOFs for the capture of highly corrosive molecules.

■ ASSOCIATED CONTENT

Supporting Information

The Supporting Information is available free of charge at https://pubs.acs.org/doi/10.1021/acs.chemmater.1c01838.

Ammonia capture by MOFs; characterization of MFM-300(Sc); ammonia adsorption studies; isosteric heat of adsorption; PXRD before and after NH_3 adsorption; adsorption isotherm of N_2 before and after NH_3 adsorption; complementary data; computational studies; DRIFT studies (PDF)

■ AUTHOR INFORMATION

Corresponding Authors

Mircea Dincă − *Department of Chemistry, Massachusetts Institute of Technology, Cambridge, Massachusetts 02139, United States;* orcid.org/0000-0002-1262-1264; Email: mdinca@mit.edu

Ilich A. Ibarra − *Laboratorio de Fisicoquímica y Reactividad de Superficies (LaFReS), Instituto de Investigaciones en Materiales, Universidad Nacional Autónoma de México, Ciudad de México 04510, México;* orcid.org/0000-0002-8573-8033; Email: argel@unam.mx; Fax: +52(55)5622-4595

Guillaume Maurin − *ICGM, Univ. Montpellier, CNRS, ENSCM, Montpellier 34095, France;* Email: guillaume.maurin1@umontpellier.fr

Authors

Pengbo Lyu − *ICGM, Univ. Montpellier, CNRS, ENSCM, Montpellier 34095, France;* orcid.org/0000-0002-1785-9861

Ashley M. Wright − *Department of Chemistry, Massachusetts Institute of Technology, Cambridge, Massachusetts 02139, United States*

Alfredo López-Olvera − *Laboratorio de Fisicoquímica y Reactividad de Superficies (LaFReS), Instituto de Investigaciones en Materiales, Universidad Nacional Autónoma de México, Ciudad de México 04510, México*

Paulo G.M. Mileo − *ICGM, Univ. Montpellier, CNRS, ENSCM, Montpellier 34095, France;* orcid.org/0000-0002-1363-7268

J. Antonio Zárate − *ICGM, Univ. Montpellier, CNRS, ENSCM, Montpellier 34095, France; Laboratorio de Fisicoquímica y Reactividad de Superficies (LaFReS), Instituto de Investigaciones en Materiales, Universidad Nacional Autónoma de México, Ciudad de México 04510, México*

Eva Martínez-Ahumada − *Laboratorio de Fisicoquímica y Reactividad de Superficies (LaFReS), Instituto de Investigaciones en Materiales, Universidad Nacional Autónoma de México, Ciudad de México 04510, México*

Vladimir Martis − *Surface Measurement Systems, London HA04PE, U.K.*

Daryl R. Williams − *Surfaces and Particle Engineering Laboratory (SPEL), Department of Chemical Engineering, Imperial College London, London SW7 2AZ, U.K.; Director of Discovery Space and Professor of Particle Science, Department of Chemical Engineering, Imperial College, London SW7 2BY, U.K.;* orcid.org/0000-0001-5626-5903

Complete contact information is available at: https://pubs.acs.org/10.1021/acs.chemmater.1c01838

Author Contributions

¶P.L., A.M.W., and A.L.-O. contributed equally to this work.

Notes

The authors declare no competing financial interest.

■ ACKNOWLEDGMENTS

I.A.I. thanks PAPIIT UNAM (IN202820), México for financial support. A.L.-O. thanks CONACYT for PhD fellowship (766200). We thank U. Winnberg (Pharma View Consulting SC) for scientific discussions and G. Ibarra-Winnberg for scientific encouragement. This work was performed using HPC resources from GENCI-CINES (grant A0100907613). This project has received funding from the European Union's Horizon 2020 research and innovation program under grant agreement no 837975.

■ REFERENCES

(1) Devic, T.; Serre, C. High Valence 3p and Transition Metal Based MOFs. *Chem. Soc. Rev.* **2014**, *43*, 6097−6115.

(2) Yuan, S.; Feng, L.; Wang, K.; Pang, J.; Bosch, M.; Lollar, C.; Sun, Y.; Qin, J.; Yang, X.; Zhang, P.; Wang, Q.; Zou, L.; Zhang, Y.; Zhang, L.; Fang, Y.; Li, J.; Zhou, H. C. Stable Metal−Organic Frameworks: Design, Synthesis, and Applications. *Adv. Mater.* **2018**, *30*, 1704303.

(3) (a) Yuan, S.; Qin, J.-S.; Lollar, C. T.; Zhou, H.-C. Stable Metal-Organic Frameworks with Group 4 Metals: Current Status and Trends. *ACS Cent. Sci.* **2018**, *4*, 440−450. (b) Mouchaham, G.; Cui, F. S.; Nouar, F.; Pimenta, V.; Chang, J.-S.; Serre, C. Metal-Organic Frameworks and Water: 'From Old Enemies to Friends'? *Trends Chem.* **2020**, *2*, 990−1003.

(4) Mouchaham, G.; Cui, F. S.; Nouar, F.; Pimenta, V.; Chang, J.-S.; Serre, C. Metal-Organic Frameworks and Water: 'From Old Enemies to Friends'? *Trends Chem.* **2020**, *2*, 990−1003.
(5) Feng, L.; Wang, K.-Y.; Day, G. S.; Ryder, M. R.; Zhou, H.-C. Destruction of Metal-Organic Frameworks: Positive and Negative Aspects of Stability and Lability. *Chem. Rev.* **2020**, *120*, 13087−13133.
(6) Feng, L.; Wang, K.-Y.; Powell, J.; Zhou, H.-C. Controllable Synthesis of Metal-Organic Frameworks and Their Hierarchical Assemblies. *Matter* **2019**, *1*, 801−824.
(7) Rao, Y.-L.; Chortos, A.; Pfattner, R.; Lissel, F.; Chiu, Y.-C.; Feig, V.; Xu, J.; Kurosawa, T.; Gu, X.; Wang, C.; He, M.; Chung, J. W.; Bao, Z. Stretchable Self-Healing Polymeric Dielectrics Cross-Linked through Metal-Ligand Coordination. *J. Am. Chem. Soc.* **2016**, *138*, 6020−6027.
(8) Williams, K. A.; Boydston, A. J.; Bielawski, C. W. Main-Chain Organometallic Polymers: Synthetic Strategies, Applications, and Perspectives. *Chem. Soc. Rev.* **2007**, *36*, 729−744.
(9) Winter, A.; Schubert, U. S. Synthesis and Characterization of Metallo-Supramolecular Polymers. *Chem. Soc. Rev.* **2016**, *45*, 5311−5357.
(10) Chakravarty, C.; Debenedetti, P. G.; Stillinger, F. H. Lindemann Measures for the Solid-Liquid Phase Transition. *J. Chem. Phys.* **2007**, *126*, 204508.
(11) Bennett, T. D.; Horike, S. Liquid, glass and amorphous solid states of coordination polymers and metal-organic frameworks. *Nat. Rev. Mater.* **2018**, *3*, 431−440.
(12) Longley, L.; Collins, S. M.; Li, S.; Smales, G. J.; Erucar, I.; Qiao, A.; Hou, J.; Doherty, C. M.; Thornton, A. W.; Hill, A. J.; Yu, X.; Terrill, N. J.; Smith, A. J.; Cohen, S. M.; Midgley, P. A.; Keen, D. A.; Telfer, S. G.; Bennett, T. D. Flux Melting of Metal-Organic Frameworks. *Chem. Sci.* **2019**, *10*, 3592−3601.
(13) Ogawa, T.; Takahashi, K.; Nagarkar, S. S.; Ohara, K.; Hong, Y.-l.; Nishiyama, Y.; Horike, S. Coordination Polymer Glass from a Protic Ionic Liquid: Proton Conductivity and Mechanical Properties as an Electrolyte. *Chem. Sci.* **2020**, *11*, 5175−5181.
(14) Andreeva, A. B.; Le, K. N.; Chen, L.; Kellman, M. E.; Hendon, C. H.; Brozek, C. K.; Hendon, C. H. Soft Mode Metal-Linker Dynamics in Carboxylate MOFs Evidenced by Variable-Temperature Infrared Spectroscopy. *J. Am. Chem. Soc.* **2020**, *142*, 19291−19299.
(15) Brozek, C. K.; Michaelis, V. K.; Ong, T.-C.; Bellarosa, L.; López, N.; Griffin, R. G.; Dincă, M. Dynamic DMF Binding in MOF-5 Enables the Formation of Metastable Cobalt-Substituted MOF-5 Analogues. *ACS Cent. Sci.* **2015**, *1*, 252−260.
(16) Brozek, C. K.; Dincă, M. Cation Exchange at the Secondary Building Units of Metal-Organic Frameworks. *Chem. Soc. Rev.* **2014**, *43*, 5456−5467.
(17) Seo, J.; Bonneau, C.; Matsuda, R.; Takata, M.; Kitagawa, S. Soft Secondary Building Unit: Dynamic Bond Rearrangement on Multinuclear Core of Porous Coordination Polymers in Gas Media. *J. Am. Chem. Soc.* **2011**, *133*, 9005−9013.
(18) Rieth, A. J.; Wright, A. M.; Dincă, M. Kinetic stability of metal-organic frameworks for corrosive and coordinating gas capture. *Nat. Rev. Mater.* **2019**, *4*, 708−725.
(19) Rieth, A. J.; Wright, A. M.; Dincă, M. Kinetic stability of metal-organic frameworks for corrosive and coordinating gas capture. *Nat. Rev. Mater.* **2019**, *4*, 708−725.
(20) Rieth, A. J.; Tulchinsky, Y.; Dincă, M. High and Reversible Ammonia Uptake in Mesoporous Azolate Metal-Organic Frameworks with Open Mn, Co, and Ni Sites. *J. Am. Chem. Soc.* **2016**, *138*, 9401−9404.
(21) Han, X.; Lu, W.; Chen, Y.; Da Silva, I.; Li, J.; Lin, L.; Li, W.; Sheveleva, A. M.; Godfrey, H. G. W.; Lu, Z.; Tuna, F.; McInnes, E. J. L.; Cheng, Y.; Daemen, L. L.; MPherson, L. J. M.; Teat, S. J.; Frogley, M. D.; Rudić, S.; Manuel, P.; Ramirez-Cuesta, A. J.; Yang, S.; Schröder, M. High Ammonia Adsorption in MFM-300 Materials: Dynamics and Charge Transfer in Host-Guest Binding. *J. Am. Chem. Soc.* **2021**, *143*, 3153−3161.
(22) Wang, Y.; Zhao, X.; Yang, H.; Bu, X.; Wang, Y.; Jia, X.; Li, J.; Feng, P. A Tale of Two Trimers from Two Different Worlds: A COF-Inspired Synthetic Strategy for Pore-Space Partitioning of MOFs. *Angew. Chem., Int. Ed.* **2019**, *58*, 6316−6320.
(23) Ibarra, I. A.; Yang, S.; Lin, X.; Blake, A. J.; Rizkallah, P. J.; Nowell, H.; Allan, D. R.; Champness, N. R.; Hubberstey, P.; Schröder, M. Highly Porous and Robust Scandium-Based Metal-Organic Frameworks for Hydrogen Storage. *Chem. Commun.* **2011**, *47*, 8304−8306.
(24) Godfrey, H. G. W.; da Silva, I.; Briggs, L.; Carter, J. H.; Morris, C. G.; Savage, M.; Easun, T. L.; Manuel, P.; Murray, C. A.; Tang, C. C.; Frogley, M. D.; Cinque, G.; Yang, S.; Schröder, M. Ammonia Storage by Reversible Host-Guest Site Exchange in a Robust Metal-Organic Framework. *Angew. Chem., Int. Ed.* **2018**, *57*, 14778−14781.
(25) Han, X.; Lu, W.; Chen, Y.; Da Silva, I.; Li, J.; Lin, L.; Li, W.; Sheveleva, A. M.; Godfrey, H. G. W.; Lu, Z.; Tuna, F.; McInnes, E. J. L.; Cheng, Y.; Daemen, L. L.; MPherson, L. J. M.; Teat, S. J.; Frogley, M. D.; Rudić, S.; Manuel, P.; Ramirez-Cuesta, A. J.; Yang, S.; Schröder, M. High Ammonia Adsorption in MFM-300 Materials: Dynamics and Charge Transfer in Host-Guest Binding. *J. Am. Chem. Soc.* **2021**, *143*, 3153−3161.
(26) Wilcox, O. T.; Fateeva, A.; Katsoulidis, A. P.; Smith, M. W.; Stone, C. A.; Rosseinsky, M. J. Acid Loaded Porphyrin-Based Metal-Organic Framework for Ammonia Uptake. *Chem. Commun.* **2015**, *51*, 14989−14991.
(27) Gonzalez, M. R.; González-Estefan, J. H.; Lara-García, H. A.; Sánchez-Camacho, P.; Basaldella, E. I.; Pfeiffer, H.; Ibarra, I. A. Separation of CO2from CH4and CO2capture in the presence of water vapour in NOTT-400. *New J. Chem.* **2015**, *39*, 2400−2403.
(28) Zárate, J. A.; Sánchez-González, E.; Williams, D. R.; González-Zamora, E.; Martis, V.; Martínez, A.; Balmaseda, J.; Maurin, G.; Ibarra, I. A. High and Energy-Efficient Reversible SO2 Uptake by a Robust Sc(III)-Based MOF. *J. Mater. Chem. A* **2019**, *7*, 15580−15584.
(29) Flores, J. G.; Zárate-Colín, J. A.; Sánchez-González, E.; Valenzuela, J. R.; Gutiérrez-Alejandre, A.; Ramírez, J.; Jancik, V.; Aguilar-Pliego, J.; Zorrilla, M. C.; Lara-García, H. A.; González-Zamora, E.; Guzmán-González, G.; González, I.; Maurin, G.; Ibarra, I. A. Partially Reversible H2S Adsorption by MFM-300(Sc): Formation of Polysulfides. *ACS Appl. Mater. Interfaces* **2020**, *12*, 18885−18892.
(30) Zhang, X.; Da Silva, I.; Godfrey, H. G. W.; Callear, S. K.; Sapchenko, S. A.; Cheng, Y.; Vitórica-Yrezábal, I.; Frogley, M. D.; Cinque, G.; Tang, C. C.; Giacobbe, C.; Dejoie, C.; Rudić, S.; Ramirez-Cuesta, A. J.; Denecke, M. A.; Yang, S.; Schröder, M. Confinement of Iodine Molecules into Triple-Helical Chains within Robust Metal-Organic Frameworks. *J. Am. Chem. Soc.* **2017**, *139*, 16289−16296.
(31) Álvarez, J. R.; Peralta, R. A.; Balmaseda, J.; González-Zamora, E.; Ibarra, I. A. Water Adsorption Properties of a Sc(III) Porous Coordination Polymer for CO2 Capture Applications. *Inorg. Chem. Front.* **2015**, *2*, 1080−1084.
(32) Osorio-Toribio, G.; Velásquez-Hernández, M. d. J.; Mileo, P. G. M.; Zárate, J. A.; Aguila-Rosas, J.; Leyva-Gómez, G.; Sánchez-Sánchez, R.; Magaña, J. J.; Pérez-Díaz, M. A.; Lázaro, I. A.; Forgan, R. S.; Maurin, G.; Lima, E.; Ibarra, I. A. Controlled Transdermal Release of Antioxidant Ferulate by a Porous Sc(III) MOF. *iScience* **2020**, *23*, 101156.
(33) Lu, E.; Li, Y.; Chen, Y. A Scandium Terminal Imido Complex: Synthesis, Structure and DFT Studies. *Chem. Commun.* **2010**, *46*, 4469−4471.
(34) Leroux, M.; Mercier, N.; Allain, M.; Dul, M.-C.; Dittmer, J.; Kassiba, A. H.; Bellat, J.-P.; Weber, G.; Bezverkhyy, I. Porous Coordination Polymer Based on Bipyridinium Carboxylate Linkers with High and Reversible Ammonia Uptake. *Inorg. Chem.* **2016**, *55*, 8587−8594.
(35) Hadjiivanov, K. I.; Panayotov, D. A.; Mihaylov, M. Y.; Ivanova, E. Z.; Chakarova, K. K.; Andonova, S. M.; Drenchev, N. L. Power of Infrared and Raman Spectroscopies to Characterize Metal-Organic Frameworks and Investigate Their Interaction with Guest Molecules. *Chem. Rev.* **2021**, *121*, 1286−1424.
(36) Kale, M. J.; Christopher, P. Utilizing Quantitative in Situ FTIR Spectroscopy to Identify Well-Coordinated Pt Atoms as the Active

https://doi.org/10.1021/acs.chemmater.1c01838
Chem. Mater. 2021, 33, 6186−6192

Site for CO Oxidation on Al2O3-Supported Pt Catalysts. *ACS Catal.* **2016**, *6*, 5599−5609.
(37) Zhang, X.; Chen, L.; Yuan, L.; Liu, R.; Li, D.; Liu, X.; Ge, G. Conformation-Dependent Coordination of Carboxylic Acids with Fe3O4 Nanoparticles Studied by ATR-FTIR Spectral Deconvolution. *Langmuir* **2019**, *35*, 5770−5778.
(38) Jayalath, S.; Wu, H.; Larsen, S. C.; Grassian, V. H. Surface Adsorption of Suwannee River Humic Acid on TiO2 Nanoparticles: A Study of pH and Particle Size. *Langmuir* **2018**, *34*, 3136−3145.
(39) Liu, F.; Song, S.; Cheng, G.; Xiong, W.; Shi, L.; Zhang, Y. MIL-101(Cr) Metal−Organic Framework Functionalized with Tetraethylenepentamine for Potential Removal of Uranium (VI) from Waste Water. *Adsorpt. Sci. Technol.* **2018**, *36*, 1550−1567.
(40) Petit, C.; Mendoza, B.; Bandosz, T. J. Reactive Adsorption of Ammonia on Cu-Based MOF/Graphene Composites. *Langmuir* **2010**, *26*, 15302−15309.
(41) Petit, C.; Levasseur, B.; Mendoza, B.; Bandosz, T. J. Reactive Adsorption of Acidic Gases on MOF/Graphite Oxide Composites. *Microporous Mesoporous Mater.* **2012**, *154*, 107−112.
(42) Petit, C.; Bandosz, T. J. Exploring the Coordination Chemistry of MOF-Graphite Oxide Composites and Their Applications as Adsorbents. *Dalton Trans.* **2012**, *41*, 4027−4035.
(43) Zeleňák, V.; Vargová, Z.; Györyová, K. Correlation of Infrared Spectra of Zinc(II) Carboxylates with Their Structures. *Spectrochim. Acta, Part A* **2007**, *66*, 262−272.
(44) Gong, Y.; Zhou, M.; Andrews, L. Spectroscopic and Theoretical Studies of Transition Metal Oxides and Dioxygen Complexes. *Chem. Rev.* **2009**, *109*, 6765−6808.
(45) Parashar, G. K.; Rai, A. K. Synthesis, Molecular Weights and Infrared Spectra of Some Scandium(III) Higher Carboxylates. *Transition Met. Chem.* **1978**, *3*, 49−50.
(46) Jiang, L.; Xu, Q. Infrared Spectroscopic and Density Functional Theory Studies on the Reactions of Zinc and Cadmium Atoms with Ammonia. *Bull. Chem. Soc. Jpn.* **2006**, *79*, 1519−1524.
(47) Griffith, W. P. Infrared and Raman Spectra of Group VIII Ammine Complexes. *J. Chem. Soc. A* **1966**, 899−901.
(48) Nakagawa, I.; Mizushima, S.-I.; Saraceno, A. J.; Lane, T. J.; Quagliano, J. V. Infrared Absorption Spectra of Inorganic Co-Ordination Complexes—XV. *Spectrochim. Acta* **1958**, *12*, 239−243.
(49) Nakagawa, I.; Mizushima, S.-I.; Saraceno, A. J.; Lane, T. J.; Quagliano, J. V. Infrared Absorption Spectra of Inorganic Co-Ordination Complexes—XV. *Spectrochim. Acta* **1958**, *12*, 239−243.
(50) Moribe, S.; Chen, Z.; Alayoglu, S.; Syed, Z. H.; Islamoglu, T.; Farha, O. K. Ammonia Capture within Isoreticular Metal-Organic Frameworks with Rod Secondary Building Units. *ACS Mater. Lett.* **2019**, *1*, 476−480.
(51) Hadjiivanov, K. *Identification and Characterization of Surface Hydroxyl Groups by Infrared Spectroscopy*, 1st ed.; Elsevier Inc., 2014; Vol. 57.
(52) Van Humbeck, J. F.; McDonald, T. M.; Jing, X.; Wiers, B. M.; Zhu, G.; Long, J. R. Ammonia Capture in Porous Organic Polymers Densely Functionalized with Brønsted Acid Groups. *J. Am. Chem. Soc.* **2014**, *136*, 2432−2440.

https://doi.org/10.1021/acs.chemmater.1c01838
Chem. Mater. 2021, 33, 6186−6192